Perfect density models cannot guarantee anomaly detection

Charline Le Lan *
Department of Statistics
University of Oxford
United Kingdom
charline.lelan@stats.ox.ac.uk

Laurent Dinh
Google Brain
laurentdinh@google.com

Abstract

Thanks to the tractability of their likelihood, some deep generative models show promise for seemingly straightforward but important applications like anomaly detection, uncertainty estimation, and active learning. However, the likelihood values empirically attributed to anomalies conflict with the expectations these proposed applications suggest. In this paper, we take a closer look at the behavior of distribution densities and show that these quantities carry less meaningful information than previously thought, beyond estimation issues or the curse of dimensionality. We conclude that the use of these likelihoods for out-of-distribution detection relies on strong and implicit hypotheses, and highlight the necessity of explicitly formulating these assumptions for reliable anomaly detection.

1 Introduction

Several machine learning methods aim at extrapolating a behavior observed on training data in order to produce predictions on new observations. But every so often, such extrapolation can result in wrong outputs, especially on points that we would consider infrequent with respect to the training distribution. Faced with unusual situations, whether adversarial (Szegedy et al., 2013; Carlini and Wagner, 2017) or just rare (Hendrycks and Dietterich, 2019), a desirable behavior from a machine learning system would be to flag these *outliers* so that the user can assess if the result is reliable and gather more information if need be (Zhao and Tresp, 2019; Fu et al., 2017). This can be critical for applications like medical decision making (Lee et al., 2018) or autonomous vehicle navigation (Filos et al., 2020), where such outliers are ubiquitous.

What are the situations that are deemed unusual? Defining these *anomalies* (Hodge and Austin, 2004; Pimentel et al., 2014) manually can be laborious if not impossible, and so generally applicable, automated methods are preferable. In that regard, the framework of *probabilistic reasoning* has been an appealing formalism because a natural candidate for outliers are situations that are *improbable* or *out-of-distribution*. Since the true *probability distribution density* p^*_X of the data is often not provided, one would instead use an estimator, $p^{(\theta)}_X$, from this data to assess the regularity of a point.

Density estimation has been a particularly challenging task on high-dimensional problems. However, recent advances in *deep probabilistic models*, including variational auto-encoders (Kingma and Welling, 2014; Rezende et al., 2014; Vahdat and Kautz, 2020), deep autoregressive models (Uria et al., 2014; van den Oord et al., 2016b,a), and flow-based generative models (Dinh et al., 2014, 2016; Kingma and Dhariwal, 2018), have shown promise for density estimation, which has the potential to enable accurate *density-based methods* (Bishop, 1994) for anomaly detection.

*Work performed while a Google Student Researcher.

1st I Can't Believe It's Not Better Workshop (ICBINB@NeurIPS 2020), Vancouver, Canada.

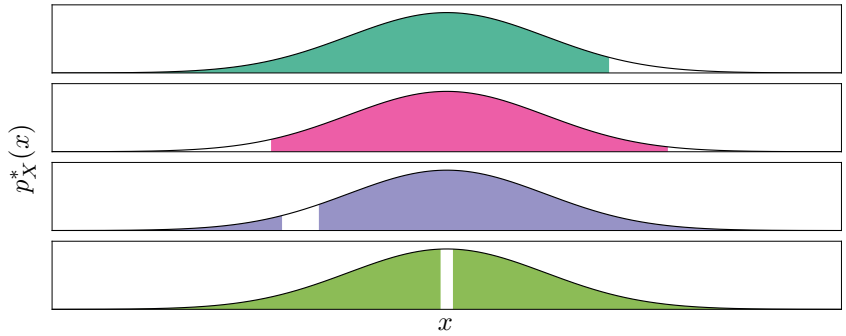

Figure 1: There is an infinite number of ways to partition a distribution in two subsets, $\mathcal{X}_{in}$ and $\mathcal{X}_{out}$ such that $P_X^*(\mathcal{X}_{in}) = 0.95$. Here, we show several choices for a standard Gaussian $p_X^* = \mathcal{N}(0, 1)$.

Yet, several works have observed that a significant gap persists between the potential of density-based anomaly detection and empirical results. For instance, Choi et al. (2018), Nalisnick et al. (2018), and Hendrycks et al. (2018) noticed that generative models trained on a benchmark dataset (e.g., CIFAR-10, Krizhevsky et al., 2009) and tested on another (e.g., SVHN, Netzer et al., 2011) are not able to identify the latter as out-of-distribution with current methods. Different hypotheses have been formulated to explain that discrepancy, ranging from the *curse of dimensionality* (Nalisnick et al., 2019) to a significant mismatch between $p_X^{(\theta)}$ and p_X^* (Choi et al., 2018; Fetaya et al., 2020; Kirichenko et al., 2020; Zhang et al., 2020; Wang et al., 2020).

In this work, we propose a new perspective on this discrepancy and challenge the expectation that density estimation should enable anomaly detection. We show that the aforementioned discrepancy persists even with perfect density models, and therefore goes beyond issues of estimation, approximation, or optimization errors (Bottou and Bousquet, 2008). We highlight that this issue is pervasive as it occurs even in low-dimensional settings and for a variety of density-based methods for anomaly detection.

2 Density-based anomaly detection

2.1 Unsupervised anomaly detection: problem statement

Unsupervised anomaly detection is a classification problem (Moya et al., 1993; Schölkopf et al., 2001), where one aims at distinguishing between regular points (*inliers*) and irregular points (*outliers*). However, as opposed to the usual classification task, labels distinguishing inliers and outliers are not provided for training, if outliers are even provided at all. Given a input space $\mathcal{X} \subseteq \mathbb{R}^D$, the task can be summarized as partitioning this space between the subset of outliers $\mathcal{X}_{out}$ and the subset of inliers $\mathcal{X}_{in}$, i.e., $\mathcal{X}_{out} \cup \mathcal{X}_{in} = \mathcal{X}$ and $\mathcal{X}_{out} \cap \mathcal{X}_{in} = \varnothing$. When the training data is distributed according to the probability measure P_X^* (with density p_X^* [1]), one would usually pick the set of regular points $\mathcal{X}_{in}$ such that this set contains the majority (but not all) of the mass (e.g., 95%) of this distribution (Schölkopf et al., 2001), i.e., $P_X^*(\mathcal{X}_{in}) = 1 - \alpha \in \left(\frac{1}{2}, 1\right)$. But, for any given α, there exists in theory an infinity of corresponding partitions into $\mathcal{X}_{in}$ and $\mathcal{X}_{out}$ (see Figure 1). How are these partitions defined to match our intuition of inliers and outliers? We will focus in this paper on recently used methods based on probability density.

2.2 Density scoring

When talking about outliers, infrequent observations, the association with probability can be quite intuitive. For instance, one would expect an anomaly to happen rarely and be unlikely. Since the language of statistics often associate the term *likelihood* with quantities like $p_X^{(\theta)}(x)$, one might consider an unlikely sample to have a low "likelihood", that is a low probability density $p_X^*(x)$. Conversely, regular samples would have a high density $p_X^*(x)$ following that reasoning. This is an intuition that is not only prevalent in several modern anomaly detection methods (Bishop, 1994; Blei

[1] We will also assume in the rest of the paper that for any $x \in \mathcal{X}, p_X^*(x) > 0$.

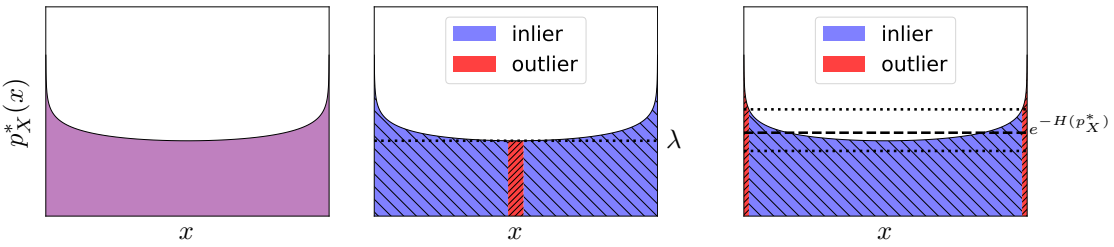

(a) An example of a distribution density p_X^*.

(b) Density scoring method applied to the distribution density p_X^*.

(c) Typicality test method (with one sample) applied to the distribution density p_X^*.

Figure 2: Illustration of different density-based methods applied to a particular one-dimensional distribution p_X^*. Outliers are in red and inliers are in blue. The thresholds are picked so that inliers include 95% of the mass. In Figure 2b, inliers are considered as the points with density above the threshold $\lambda > 0$ while in Figure 2c, they are the points whose log-density are in the ϵ-interval around the negentropy $-H(p_X^*)$.

et al., 2017; Hendrycks et al., 2018; Kirichenko et al., 2020; Rudolph et al., 2020; Liu et al., 2020) but also in techniques like low-temperature sampling (Graves, 2013) used for example in Kingma and Dhariwal (2018) and Parmar et al. (2018).

The associated approach, described in Bishop (1994), consists in defining the inliers as the points whose density exceed a certain threshold $\lambda > 0$ (for example, chosen such that inliers include a predefined amount of mass, e.g., 95%), making the modes the most regular points in this setting. $\mathcal{X}_{out}$ and $\mathcal{X}_{in}$ are then respectively the lower-level and upper-level sets $\{x \in \mathcal{X}, p_X^*(x) \leq \lambda\}$ and $\{x \in \mathcal{X}, p_X^*(x) > \lambda\}$ (see Figure 2b).

2.3 Typicality Test

The *Gaussian Annulus theorem* (Blum et al., 2016) (generalized in Vershynin, 2019) attests that most of the mass of a high-dimensional standard Gaussian $\mathcal{N}(0, \mathbb{I}_D)$ is located close to the hypersphere of radius $\sqrt{D}$. However, the mode of its density is at the center 0. A natural conclusion is that the *curse of dimensionality* creates a discrepancy between the density upper-level sets and what we expect as inliers (Choi et al., 2018; Nalisnick et al., 2019; Morningstar et al., 2020; Dieleman, 2020). This motivated Nalisnick et al. (2019) to propose another method for testing whether a point is an inlier or not, relying on a measure of its *typicality*. This method relies on the notion of *typical set* (Cover, 1999) defined by taking as inliers points whose average log-density is close to the average log-density of the distribution (see Figure 2c).

Definition 1 (Cover, 1999)**.** *Given independent and identically distributed elements $\left(x^{(n)}\right)_{n \leq N}$ from a distribution with density p_X^*, the typical set $A_\epsilon^{(N)}(p_X^*) \subset \mathcal{X}^N$ is made of all sequences that satisfy:*

$$\left| H(p_X^*) + \frac{1}{N} \sum_{n=1}^{N} \log p_X^* \left(x^{(n)}\right) \right| \leq \epsilon,$$

where $H(X) = -\mathbb{E}[\log p_X^*(X)]$ is the (differential) entropy and $\epsilon > 0$ a constant.

This method matches the intuition behind the Gaussian Annulus theorem on the set of inliers of a high-dimensional standard Gaussian. Indeed, using a concentration inequality, we can show that $\lim_{N \to +\infty} \left(P^*_{(X_i)_{1 \leq n \leq N}} \left(A_\epsilon^{(N)} \right) \right) = 1$, which means that with N large enough, $A_\epsilon^{(N)}(p_X^*)$ will contain most of the mass of $(p_X^*)^N$, justifying the name *typicality*.

3 The role of reparametrization

Given the anomaly detection problem formulation Subsection 2.1, we are interested in reasoning about the properties a solution ought to satisfy, in the ideal case of infinite data and capacity. Under these conditions, a reasonable algorithm should, in every possible case considered, converge to the right solution. In deep learning, the development of universal approximation theorems (Cybenko, 1989; Hornik, 1991; Pinkus, 1999) and the use of proper scoring rule follow these considerations for example. As density-based methods rely on density estimation, we will assume that $p_X^{(\theta)} = p_X^*$ under infinite data and capacity. This is an appealing setting as it gives space for theoretical results without worrying about the underfitting or overfitting issues mentioned by Hendrycks et al. (2018); Fetaya et al. (2020); Morningstar et al. (2020); Kirichenko et al. (2020); Zhang et al. (2020).

Although we work in practice on points (e.g., vectors), it is important to keep in mind that these points are actually representations of an underlying outcome. As a random variable, X is by definition the function from this outcome ω to the corresponding observation $x = X(\omega)$. However, at its core, an anomaly detection solution aims at classifying (without supervision) outcomes through these measurements. How is the choice of X affecting the problem of anomaly detection? While several papers studied the effects of a change of representation through the lens of inductive bias (Kirichenko et al., 2020; Zhang et al., 2020), we investigate the more fundamental effects of reparametrizations f. To sidestep concerns about loss of information (Winkens et al., 2020), we study the particular case of an invertible map f.

An example of invertible map is the change of coordinate system from Cartesian $(x_i)_{i \leq D}$ to hyperspherical, consisting of a radial coordinate $r > 0$ and $(D-1)$ angular coordinates $(\phi_i)_{i<D}$,

$$\forall d < D,\ x_d = r \left(\prod_{i=1}^{d-1} \sin(\phi_i) \right) \cos(\phi_d)$$
$$x_D = r \left(\prod_{i=1}^{D-2} \sin(\phi_i) \right) \sin(\phi_{D-1}),$$

where for all $i \in \{1, 2, ..., D-2\}$, $\phi_i \in [0, \pi)$ and $\phi_{D-1} \in [0, 2\pi)$. While significantly different, those two systems of coordinates (or representations) describe the same vector.

Similarly, for f invertible, the measurements $x = X(\omega)$ and $f(x) = (f \circ X)(\omega)$ represent the same outcome ω (although differently), and, since x and $f(x)$ are connected by an invertible transformation f, the same method applied respectively to X or $f(X)$ should classify them with the same label, either as an inlier or an outlier. The target of these methods is to essentially assess the regularity of the outcome ω. From this, we could ideally make the following requirement for a solution to anomaly detection.

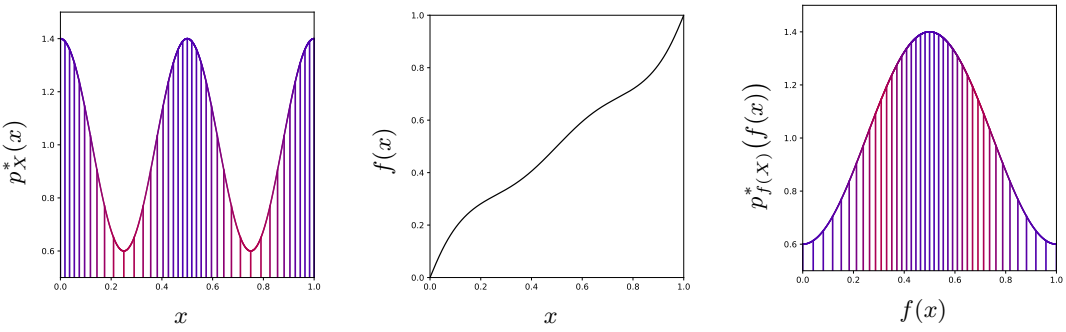

(a) An example of a distribution density p_X^*.

(b) Example of an invertible function f from $[0, 1]$ to $[0, 1]$.

(c) Resulting density $p_{f(X)}^*$ from applying f to $X \sim p_X^*$ as a function of the new axis $f(x)$.

Figure 3: Illustration of the change of variables formula and how much the application of a bijection can affect the density of the points considered in a one-dimensional case. In Figures 3a and 3c, points x with high density $p_X^*(x)$ are in blue and points with low density $p_X^*(x)$ are in red.

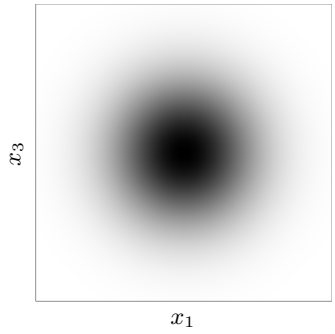

(a) A three-dimensional standard Gaussian distribution density in Cartesian coordinates on the hyperplane defined by $x_2 = 0$.

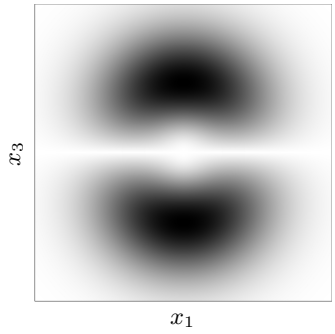

(b) A three-dimensional standard Gaussian distribution density in hyperspherical coordinates (plotted in Cartesian coordinates) on the hyperplane defined by $x_2 = 0$.

Figure 4: Illustration of the change of variables formula for a three-dimensional standard Gaussian distribution with a change of coordinate system, from Cartesian to hyperspherical.

Principle. *In an infinite data and capacity setting, the result of an anomaly detection method should be invariant to any continuous invertible reparametrization f.*

Do density-based methods follow this principle? To answer that question, we look into how density behaves under a reversible change of representation. In particular, the change of variables formula (Kaplan, 1952) (used in Tabak and Turner, 2013; Dinh et al., 2014; Rezende and Mohamed, 2015), formalizes a simple intuition of this behavior: where points are brought closer together the density increases whereas this density decreases when points are spread apart. The formula itself is written as:

$$p^*_{f(X)}\big(f(x)\big) = p^*_X(x) \left| \frac{\partial f}{\partial x^T}(x) \right|^{-1},$$

where $\left| \frac{\partial f}{\partial x^T}(x) \right|$ is the Jacobian determinant of f at x, a quantity that reflects a local change in volume incurred by f. Figure 3 already illustrates how the function f (Figure 3b) can spread apart points close to the extremities to decrease the corresponding density round 0 and 1, and, as a result, turns the density on the left (Figure 3a) into the density on the right (Figure 3c). Figure 4 shows how much a simple change of coordinate system, from Cartesian (Figure 4a) to hyperspherical (Figure 4b), can significantly affect the resulting density associated to a point. This comes from the Jacobian determinant of this change of coordinates:

$$r^{D-1} \left(\prod_{d=1}^{D-1} \big(\sin(\phi_d) \big)^{D-d-1} \right).$$

With these examples, one can wonder to which degree an invertible change of representation can affect the density and the anomaly detection methods presented in Subsections 2.2 and 2.3 that use it.

4 Leveraging the change of variables formula

4.1 Uniformization

We start by showing that unambiguously defining outliers and inliers with any density-based approach becomes impossible when considering a particular type of invertible reparametrization of the problem, irrespective of dimensionality.

Under weak assumptions, one can map any distribution to a uniform distribution using an invertible transformation (Hyvärinen and Pajunen, 1999). This is in fact a common strategy for sampling from complicated one-dimensional distributions (Devroye, 1986). Figure 5 shows an example of this where a bimodal distribution (Figure 5a) is pushed through an invertible map (Figure 5b) to obtain a uniform distribution (Figure 5c).

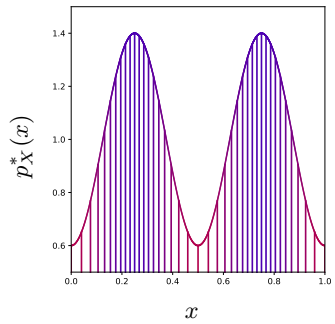

(a) An example of a distribution density p^*_X. Points x with high density $p^*_X(x)$ are in blue and points with low density $p^*_X(x)$ are in red.

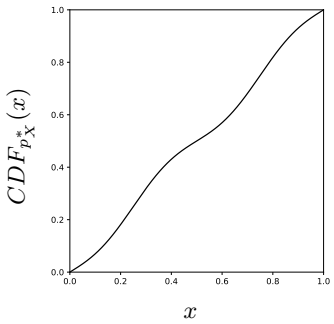

(b) The corresponding cumulative distribution function $CDF_{p^*_X}$.

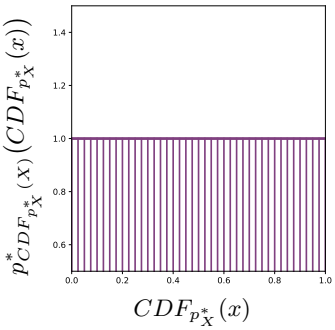

(c) The resulting density from applying $CDF_{p^*_X}$ to $X \sim p^*_X$ is $p^*_{CDF_{p^*_X}(X)} = \mathcal{U}([0,1])$, therefore we color all the points the same.

Figure 5: Illustration of the one-dimensional case version of a Knothe-Rosenblatt rearrangement, which is just the application of the cumulative distribution function $CDF_{p^*_X}$ on the variable x.

To construct this invertible uniformization function, we rely on the notion of Knothe-Rosenblatt rearrangement (Rosenblatt, 1952; Knothe et al., 1957). A Knothe-Rosenblatt rearrangement (notably used in Hyvärinen and Pajunen, 1999) is defined for a random variable X distributed according to a strictly positive density p^*_X with a convex support $\mathcal{X}$, as a continuous invertible map $f^{(KR)}$ from $\mathcal{X}$ onto $[0,1]^D$ such that $f^{(KR)}(X)$ follows a uniform distribution in this hypercube. This rearrangement is constructed as follows: $\forall d \in \{1, ..., D\}, f^{(KR)}(x) = CDF_{p^*_{X_d|X_{<d}}}(x_d \mid x_{<d})$ where CDF_p is the cumulative distribution function corresponding to the density p.

In these new coordinates, neither the density scoring method nor the typicality test approach can discriminate between inliers and outliers in this uniform D-dimensional hypercube $[0,1]^D$. Since the resulting density $p^*_{f^{(KR)}(X)} = 1$ is constant, the density scoring method attributes the same regularity to every point. Moreover, a typicality test on $f^{(KR)}(X)$ will always succeed as

$$\forall \epsilon > 0, N \in \mathbb{N}^*, \forall \left(x^{(n)}\right)_{n \leq N}, \quad \left| H\left(p^*_{f^{(KR)}(X)}\right) + \frac{1}{N}\sum_{n=1}^{N} \log p^*_{f^{(KR)}(X)}\left(f^{(KR)}\left(x^{(n)}\right)\right)\right|$$
$$= \left| H\left(\mathcal{U}\left([0,1]^D\right)\right) + \frac{1}{N}\sum_{n=1}^{N} \log(1)\right| = 0 \leq \epsilon.$$

However, these uniformly distributed points are merely a different representation of the same initial points. Therefore, if the identity of the outliers is ambiguous in this uniform distribution, then anomaly detection in general should be as difficult.

4.2 Arbitrary scoring

While a particular parametrization can prevent density-based outlier detection methods from separating between outliers and inliers, we find that it is also possible to build a reparametrization of the problem to impose to each point an arbitrary density level in the new representation. To illustrate this idea, consider some points from a distribution whose density is depicted in Figure 6a and a score function indicated in red in Figure 6b. In this example, high-density regions correspond to areas with low score value (and vice-versa). We show that there exists a reparametrization (depicted in Figure 6c) such that the density in this new representation (Figure 6d) now matches the desired score, which can be designed to mislead density-based methods into a wrong classification of anomalies.

Proposition 1. *For any variable $X \sim p^*_X$ with p^*_X continuous strictly positive (with $\mathcal{X}$ convex) and any measurable continuous function $s : \mathcal{X} \to \mathbb{R}^*_+$ bounded below by a strictly positive number, there exists a continuous bijection $f^{(s)}$ such that for any $x \in \mathcal{X}, p_{f^{(s)}(X)}\left(f^{(s)}(x)\right) = s(x)$.*

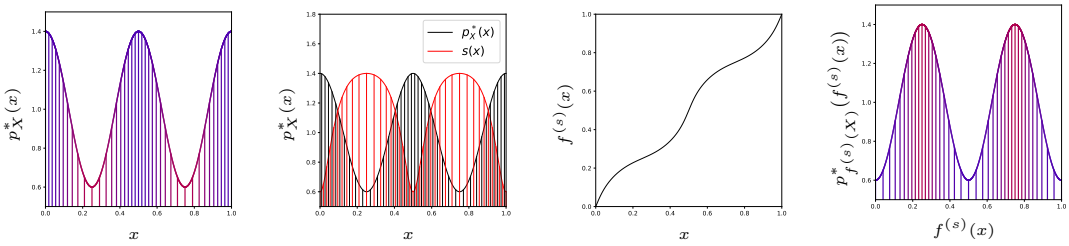

(a) An example of a distribution density p^*_X.

(b) The distribution p^*_X (in black) and the desired density scoring s (in red).

(c) A continuous invertible reparametrization $f^{(s)}$ such that $p^*_{f^{(s)}(X)}\big(f^{(s)}(x)\big) = s(x)$.

(d) Resulting density $p^*_{f^{(s)}(X)}$ from applying $f^{(s)}$ to $X \sim p^*_X$ as a function of $f^{(s)}(x)$.

Figure 6: Illustration of how we can modify the space with an invertible function so that each point x follows a predefined score. In Figures 6a and 6d, points x with high density $p^*_X(x)$ are in blue and points with low density $p^*_X(x)$ are in red.

Proof. We write x to denote $(x_1, \ldots, x_{D-1}, x_D)$ and $(x_{<D}, t)$ for $(x_1, \ldots, x_{D-1}, t)$. Let $f^{(s)} : \mathcal{X} \to \mathcal{Z} \subset \mathbb{R}^D$ be a function such that

$$\big(f^{(s)}(x)\big)_D = \int_0^{x_D} \frac{p^*_X\big((x_{<D}, t)\big)}{s\big((x_{<D}, t)\big)} dt,$$

and $\forall d \in \{1, ..., D-1\}, \big(f^{(s)}(x)\big)_d = x_d$. As s is bounded below, $f^{(s)}$ is well defined and invertible. By the change of variables formula,

$$\forall x \in \mathcal{X},\ p^*_{f^{(s)}(X)}\big(f^{(s)}(x)\big) = p^*_X(x) \cdot \left|\frac{\partial f^{(s)}}{\partial x^T}(x)\right|^{-1} = p^*_X(x) \cdot \left(\frac{p^*_X(x)}{s(x)}\right)^{-1} = s(x).$$

□

If $\mathcal{X}_{in}$ and $\mathcal{X}_{out}$ are respectively the true sets of inliers and outliers, we can pick a ball $A \subset \mathcal{X}_{in}$ such that $P^*_X(A) = \alpha < 0.5$, we can choose s such that for any $x \in (\mathcal{X} \setminus A), s(x) = 1$ and for any $x \in A, s(x) = 0.1$. With this choice of s (or a smooth approximation) and the function $f^{(s)}$ defined earlier, both the density scoring and the (one-sample) typical set methods will consider the set of inliers to be $(\mathcal{X} \setminus A)$ while $\mathcal{X}_{out} \subset (\mathcal{X} \setminus A)$, making their results completely wrong. While we can also reparametrize the problem so that these methods may succeed, such reparametrization requires knowledge of $(p^*_X/s)(x)$. Without any constraints on the space considered, individual densities can be arbitrarily manipulated, which reveals how little these quantities say about the underlying outcome in general.

4.3 Canonical distribution

Since our analysis in Subsections 4.1 and 4.2 reveals that densities or low typicality regions are not sufficient conditions for an observation to be an anomaly, whatever its distribution or its dimension, we are now interested in investigating whether additional realistic assumptions can lead to some guarantees for anomaly detection. Motivated by several representation learning algorithms which attempt to learn a mapping to a predefined distribution (e.g., a standard Gaussian, see Chen and Gopinath, 2001; Kingma and Welling, 2014; Rezende et al., 2014; Dinh et al., 2014; Krusinga et al., 2019) we consider the more restricted setting of a fixed distribution of our choice, whose regular regions could for instance be known. Surprisingly, we find that it is possible to exchange the densities of an inlier and an outlier even within a canonical distribution.

Proposition 2. *For any strictly positive density function p^*_X over a convex space $\mathcal{X} \subseteq \mathbb{R}^D$ with $D \geq 2$, for any x_{in}, x_{out} in the interior $\mathcal{X}^\circ$ of $\mathcal{X}$, there exists a continuous bijection $f : \mathcal{X} \to \mathcal{X}$ such that $p^*_X = p^*_{f(X)}$, $p^*_{f(X)}\left(f\left(x^{(in)}\right)\right) = p^*_X\left(x^{(out)}\right)$, and $p^*_{f(X)}\left(f\left(x^{(out)}\right)\right) = p^*_X\left(x^{(in)}\right)$.*

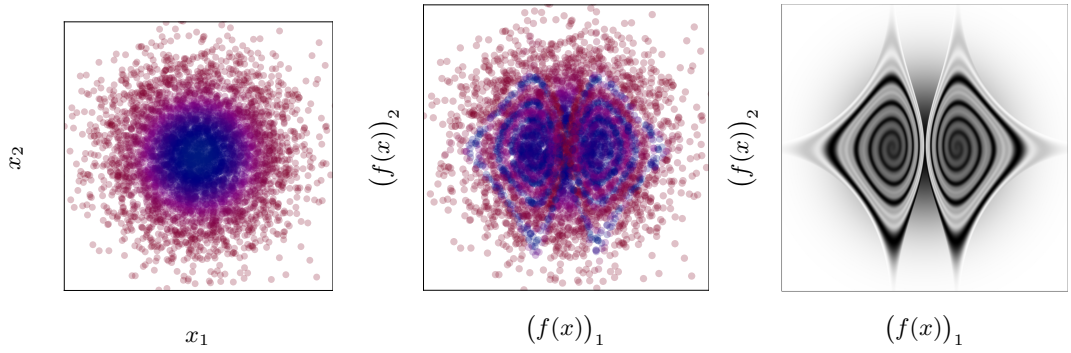

(a) Points sampled from $p^*_X = \mathcal{N}(0, \mathbb{I}_2)$.

(b) Applying a bijection f that preserves the distribution $p^*_{f(X)} = \mathcal{N}(0, \mathbb{I}_2)$ to the points in Figure 7a.

(c) The original distribution p^*_X with respect to the new coordinates $f(x)$, $p^*_X \circ f^{-1}$.

Figure 7: Application of a transformation using the bijection in Figure 8 to a standard Gaussian distribution $\mathcal{N}(0, \mathbb{I}_2)$, leaving it overall invariant.

We provide a sketch of proof and the detailed proof in Appendix A.

Since the resulting distribution $p^*_{f(X)}$ is identical to the original f^*_X, then their entropies are the same $H\left(p^*_{f(X)}\right) = H\left(f^*_X\right)$. Hence, when x_{in} and x_{out} are respectively an inlier and an outlier, whether in terms of density scoring or typicality, there exists a reparametrization of the problem conserving the overall distribution while still exchanging their status as inlier/outlier. We provide an example applied to a standard Gaussian distribution in Figure 7.

This result is important from a representation learning perspective and a complement to the general non-identifiability result in several representation learning approaches (Hyvärinen and Pajunen, 1999; Locatello et al., 2019). It means that learning a representation with a predefined, well-known distribution and knowing the true density p^*_X are not sufficient conditions to control the individual density of each point and accurately distinguish outliers from inliers.

5 Discussion

Fundamentally, density-based methods for anomaly detection rely on the belief that density, as a quantity, conveys useful information to assess whether an outcome is an outlier or not. For example, several density-based methods operate in practice on features learned independently from the anomaly detection task (Lee et al., 2018; Krusinga et al., 2019; Morningstar et al., 2020; Winkens et al., 2020) or on the original input features (Nalisnick et al., 2018; Hendrycks et al., 2018; Kirichenko et al., 2020; Rudolph et al., 2020; Nalisnick et al., 2019). In general, there is no evidence that the density in these representations will carry any useful information for anomaly detection bringing into question whether performance of probabilistic models on this task (e.g., Du and Mordatch, 2019; Grathwohl et al., 2019; Kirichenko et al., 2020; Liu and Abbeel, 2020) reflects goodness-of-fit of the density model. On the contrary, we have proven in this paper that density-based anomaly detection methods are inconsistent across a range of possible representations [2], even under strong constraints on the distribution, which suggests that finding the right input representation for meaningful density-based anomaly detection requires privileged information, as discussed in Subsection 4.2. Moreover, several papers have pointed to existing problems in commonly used input representations; for example, the geometry of a bitmap representation does not follow our intuition of semantic distance (Theis et al., 2016), or images can come from photographic sensors tuned to specific populations (Roth, 2009; Buolamwini and Gebru, 2018). This shows how strong of an otherwise understated assumption it is to suppose that the methods presented in Subsection 2.2 and Subsection 2.3 would work on input representations (see Appendix B for a simple counter-example in a bitmap representation). This is

[2] Alternatively, this can be seen as a change of base distribution used to define a probability density as a Radon-Nikodym derivative.

particularly problematic for applications as critical as autonomous vehicle navigation or medical decision-making.

While defining anomalies might be impossible without prior knowledge (Winkens et al., 2020) as out-of-distribution detection is an ill-posed problem (Choi et al., 2018; Nalisnick et al., 2019; Morningstar et al., 2020), several approaches make these assumptions more explicit. For instance, the density scoring method has also been interpreted in Bishop (1994) as a likelihood ratio method (Ren et al., 2019; Serrà et al., 2020; Schirrmeister et al., 2020), which is not only invariant to reparametrization but also more transparent with respect to its underlying assumptions. Inspired by the Bayesian approach from Choi et al. (2018), one can also work on defining a prior distribution on possible reparametrizations over which to average (similarly to Jørgensen and Hauberg, 2020).

Acknowledgements

The authors would like to thank Kyle Kastner, Johanna Hansen, Ben Poole, Arthur Gretton, Durk Kingma, Samy Bengio, Jascha Sohl-Dickstein, Polina Kirichenko, Pavel Izmailov, Ross Goroshin, Hugo Larochelle, Jörn-Henrik Jacobsen, and Kyunghyun Cho for initial discussions for this paper. We also thank Eric Jang, Alex Alemi, and the anonymous reviewers for useful feedback on this paper.

We would also like to thank the Python community (Van Rossum and Drake Jr, 1995; Oliphant, 2007) for developing the tools that enabled this work, including NumPy (Oliphant, 2006; Walt et al., 2011; Harris et al., 2020), SciPy (Jones et al., 2001), and Matplotlib (Hunter, 2007).

References

Bishop, C. M. (1994). Novelty detection and neural network validation. *IEE Proceedings-Vision, Image and Signal processing*, 141(4):217–222.

Blei, D., Heller, K., Salimans, T., Welling, M., , and Ghahramani, Z. (2017). Panel: On the foundations and future of approximate inference. In *Symposium on Advances in Approximate Bayesian Inference, AABI 2017*.

Blum, A., Hopcroft, J., and Kannan, R. (2016). Foundations of data science. *Vorabversion eines Lehrbuchs*, 5.

Bottou, L. and Bousquet, O. (2008). The tradeoffs of large scale learning. In *Advances in neural information processing systems*, pages 161–168.

Buolamwini, J. and Gebru, T. (2018). Gender shades: Intersectional accuracy disparities in commercial gender classification. In *Conference on fairness, accountability and transparency*, pages 77–91.

Carlini, N. and Wagner, D. (2017). Adversarial examples are not easily detected: Bypassing ten detection methods. In *Proceedings of the 10th ACM Workshop on Artificial Intelligence and Security*, pages 3–14.

Chen, S. S. and Gopinath, R. A. (2001). Gaussianization. In Leen, T. K., Dietterich, T. G., and Tresp, V., editors, *Advances in Neural Information Processing Systems 13*, pages 423–429. MIT Press.

Choi, H., Jang, E., and Alemi, A. A. (2018). Waic, but why? generative ensembles for robust anomaly detection. *arXiv preprint arXiv:1810.01392*.

Cover, T. M. (1999). *Elements of information theory*. John Wiley & Sons.

Cybenko, G. (1989). Approximation by superpositions of a sigmoidal function. *Mathematics of Control, Signals, and Systems (MCSS)*, 2(4):303–314.

Devroye, L. (1986). Sample-based non-uniform random variate generation. In *Proceedings of the 18th conference on Winter simulation*, pages 260–265. ACM.

Dieleman, S. (2020). Musings on typicality.

Dinh, L., Krueger, D., and Bengio, Y. (2014). Nice: Non-linear independent components estimation. *arXiv preprint arXiv:1410.8516*.

Dinh, L., Sohl-Dickstein, J., and Bengio, S. (2016). Density estimation using real nvp. *arXiv preprint arXiv:1605.08803*.

Du, Y. and Mordatch, I. (2019). Implicit generation and modeling with energy based models. In *Advances in Neural Information Processing Systems*, pages 3608–3618.

Fetaya, E., Jacobsen, J.-H., Grathwohl, W., and Zemel, R. (2020). Understanding the limitations of conditional generative models. In *International Conference on Learning Representations*.

Filos, A., Tigas, P., McAllister, R., Rhinehart, N., Levine, S., and Gal, Y. (2020). Can autonomous vehicles identify, recover from, and adapt to distribution shifts? *arXiv preprint arXiv:2006.14911*.

Fu, J., Co-Reyes, J., and Levine, S. (2017). Ex2: Exploration with exemplar models for deep reinforcement learning. In *Advances in neural information processing systems*, pages 2577–2587.

Grathwohl, W., Wang, K.-C., Jacobsen, J.-H., Duvenaud, D., Norouzi, M., and Swersky, K. (2019). Your classifier is secretly an energy based model and you should treat it like one. *arXiv preprint arXiv:1912.03263*.

Graves, A. (2013). Generating sequences with recurrent neural networks. *arXiv preprint arXiv:1308.0850*.

Harris, C. R., Millman, K. J., van der Walt, S. J., Gommers, R., Virtanen, P., Cournapeau, D., Wieser, E., Taylor, J., Berg, S., Smith, N. J., et al. (2020). Array programming with numpy. *Nature*, 585(7825):357–362.

Hendrycks, D. and Dietterich, T. (2019). Benchmarking neural network robustness to common corruptions and perturbations. In *International Conference on Learning Representations*.

Hendrycks, D., Mazeika, M., and Dietterich, T. (2018). Deep anomaly detection with outlier exposure. *arXiv preprint arXiv:1812.04606*.

Hodge, V. and Austin, J. (2004). A survey of outlier detection methodologies. *Artificial intelligence review*, 22(2):85–126.

Hornik, K. (1991). Approximation capabilities of multilayer feedforward networks. *Neural networks*, 4(2):251–257.

Hunter, J. D. (2007). Matplotlib: A 2d graphics environment. *Computing in science & engineering*, 9(3):90–95.

Hyvärinen, A. and Pajunen, P. (1999). Nonlinear independent component analysis: Existence and uniqueness results. *Neural networks*, 12(3):429–439.

Jones, E., Oliphant, T., Peterson, P., et al. (2001). Scipy: Open source scientific tools for python.

Jørgensen, M. and Hauberg, S. (2020). Reparametrization invariance in non-parametric causal discovery. *arXiv preprint arXiv:2008.05552*.

Kaplan, W. (1952). *Advanced calculus*. Pearson Education India.

Kingma, D. P. and Dhariwal, P. (2018). Glow: Generative flow with invertible 1x1 convolutions. In *Advances in neural information processing systems*, pages 10215–10224.

Kingma, D. P. and Welling, M. (2014). Auto-encoding variational bayes. In *ICLR'2014, arXiv:1312.6114*.

Kirichenko, P., Izmailov, P., and Wilson, A. G. (2020). Why normalizing flows fail to detect out-of-distribution data. *arXiv preprint arXiv:2006.08545*.

Knothe, H. et al. (1957). Contributions to the theory of convex bodies. *The Michigan Mathematical Journal*, 4(1):39–52.

Krizhevsky, A., Hinton, G., et al. (2009). Learning multiple layers of features from tiny images.

Krusinga, R., Shah, S., Zwicker, M., Goldstein, T., and Jacobs, D. (2019). Understanding the (un) interpretability of natural image distributions using generative models. *arXiv preprint arXiv:1901.01499*.

Lee, K., Lee, K., Lee, H., and Shin, J. (2018). A simple unified framework for detecting out-of-distribution samples and adversarial attacks. In *Advances in Neural Information Processing Systems*, pages 7167–7177.

Liu, H. and Abbeel, P. (2020). Hybrid discriminative-generative training via contrastive learning. *arXiv preprint arXiv:2007.09070*.

Liu, W., Wang, X., Owens, J., and Li, Y. (2020). Energy-based out-of-distribution detection. *Advances in Neural Information Processing Systems (NeurIPS)*.

Locatello, F., Bauer, S., Lucic, M., Raetsch, G., Gelly, S., Schölkopf, B., and Bachem, O. (2019). Challenging common assumptions in the unsupervised learning of disentangled representations. In *international conference on machine learning*, pages 4114–4124.

Morningstar, W. R., Ham, C., Gallagher, A. G., Lakshminarayanan, B., Alemi, A. A., and Dillon, J. V. (2020). Density of states estimation for out-of-distribution detection. *arXiv preprint arXiv:2006.09273*.

Moya, M. M., Koch, M. W., and Hostetler, L. D. (1993). One-class classifier networks for target recognition applications. *STIN*, 93:24043.

Nalisnick, E., Matsukawa, A., Teh, Y. W., Gorur, D., and Lakshminarayanan, B. (2018). Do deep generative models know what they don't know? *arXiv preprint arXiv:1810.09136*.

Nalisnick, E., Matsukawa, A., Teh, Y. W., and Lakshminarayanan, B. (2019). Detecting out-of-distribution inputs to deep generative models using typicality. *arXiv preprint arXiv:1906.02994*.

Netzer, Y., Wang, T., Coates, A., Bissacco, A., Wu, B., and Ng, A. Y. (2011). Reading digits in natural images with unsupervised feature learning.

Oliphant, T. E. (2006). *A guide to NumPy*, volume 1. Trelgol Publishing USA.

Oliphant, T. E. (2007). Python for scientific computing. *Computing in Science & Engineering*, 9(3):10–20.

Parmar, N., Vaswani, A., Uszkoreit, J., Kaiser, L., Shazeer, N., Ku, A., and Tran, D. (2018). Image transformer. Proceedings of Machine Learning Research, pages 4055–4064, Stockholmsmässan, Stockholm Sweden. PMLR.

Pimentel, M. A., Clifton, D. A., Clifton, L., and Tarassenko, L. (2014). A review of novelty detection. *Signal Processing*, 99:215–249.

Pinkus, A. (1999). Approximation theory of the mlp model in neural networks. *Acta numerica*, 8(1):143–195.

Ren, J., Liu, P. J., Fertig, E., Snoek, J., Poplin, R., Depristo, M., Dillon, J., and Lakshminarayanan, B. (2019). Likelihood ratios for out-of-distribution detection. In *Advances in Neural Information Processing Systems*, pages 14707–14718.

Rezende, D. and Mohamed, S. (2015). Variational inference with normalizing flows. In *Proceedings of Machine Learning Research*.

Rezende, D. J., Mohamed, S., and Wierstra, D. (2014). Stochastic backpropagation and approximate inference in deep generative models. In *Proceedings of Machine Learning Research*.

Rosenblatt, M. (1952). Remarks on a multivariate transformation. *The annals of mathematical statistics*, 23(3):470–472.

Roth, L. (2009). Looking at shirley, the ultimate norm: Colour balance, image technologies, and cognitive equity. *Canadian Journal of Communication*, 34(1).

Rudolph, M., Wandt, B., and Rosenhahn, B. (2020). Same same but differnet: Semi-supervised defect detection with normalizing flows. *arXiv preprint arXiv:2008.12577*.

Schirrmeister, R. T., Zhou, Y., Ball, T., and Zhang, D. (2020). Understanding anomaly detection with deep invertible networks through hierarchies of distributions and features. *arXiv preprint arXiv:2006.10848*.

Schölkopf, B., Platt, J. C., Shawe-Taylor, J., Smola, A. J., and Williamson, R. C. (2001). Estimating the support of a high-dimensional distribution. *Neural computation*, 13(7):1443–1471.

Serrà, J., Álvarez, D., Gómez, V., Slizovskaia, O., Núñez, J. F., and Luque, J. (2020). Input complexity and out-of-distribution detection with likelihood-based generative models. In *International Conference on Learning Representations*.

Szegedy, C., Zaremba, W., Sutskever, I., Bruna, J., Erhan, D., Goodfellow, I., and Fergus, R. (2013). Intriguing properties of neural networks. *arXiv preprint arXiv:1312.6199*.

Tabak, E. G. and Turner, C. V. (2013). A family of nonparametric density estimation algorithms. *Communications on Pure and Applied Mathematics*, 66(2):145–164.

Theis, L., van den Oord, A., and Bethge, M. (2016). A note on the evaluation of generative models. In *ICLR'2016 arXiv:1511.01844*.

Uria, B., Murray, I., and Larochelle, H. (2014). A deep and tractable density estimator. In *International Conference on Machine Learning*, pages 467–475.

Vahdat, A. and Kautz, J. (2020). Nvae: A deep hierarchical variational autoencoder. *arXiv preprint arXiv:2007.03898*.

van den Oord, A., Kalchbrenner, N., Espeholt, L., Vinyals, O., Graves, A., et al. (2016a). Conditional image generation with pixelcnn decoders. In *Advances in Neural Information Processing Systems*, pages 4790–4798.

van den Oord, A., Kalchbrenner, N., and Kavukcuoglu, K. (2016b). Pixel recurrent neural networks. In *International Conference on Machine Learning*, pages 1747–1756.

Van Rossum, G. and Drake Jr, F. L. (1995). *Python reference manual*. Centrum voor Wiskunde en Informatica Amsterdam.

Vershynin, R. (2019). High-dimensional probability.

Walt, S. v. d., Colbert, S. C., and Varoquaux, G. (2011). The numpy array: a structure for efficient numerical computation. *Computing in science & engineering*, 13(2):22–30.

Wang, Z., Dai, B., Wipf, D., and Zhu, J. (2020). Further analysis of outlier detection with deep generative models. *Advances in Neural Information Processing Systems*, 33.

Winkens, J., Bunel, R., Roy, A. G., Stanforth, R., Natarajan, V., Ledsam, J. R., MacWilliams, P., Kohli, P., Karthikesalingam, A., Kohl, S., et al. (2020). Contrastive training for improved out-of-distribution detection. *arXiv preprint arXiv:2007.05566*.

Zhang, H., Li, A., Guo, J., and Guo, Y. (2020). Hybrid models for open set recognition. *arXiv preprint arXiv:2003.12506*.

Zhao, R. and Tresp, V. (2019). Curiosity-driven experience prioritization via density estimation. *arXiv preprint arXiv:1902.08039*.

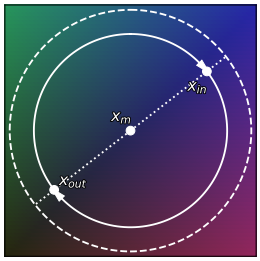

(a) Points x_{in} and x_{out} in a uniformly distributed subset. $f^{(rot)}$ will pick a two-dimensional plane and use the polar coordinate using the mean x_m of x_{in} and x_{out} as the center.

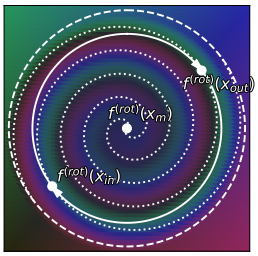

(b) Applying a bijection $f^{(rot)}$ exchanging the points x_{in} and x_{out}. $f^{(rot)}$ is a rotation depending on the distance from the mean x_m of x_{in} and x_{out} in the previously selected two-dimensional plane.

Figure 8: Illustration of the norm-dependent rotation, a locally-acting bijection that allows us to swap two different points while preserving a uniform distribution (as a volume-preserving function).

A Proof of Proposition 2

Proposition 3. *For any strictly positive density function p_X^* over a convex space $\mathcal{X} \subseteq \mathbb{R}^D$ with $D > 2$, for any x_{in}, x_{out} in the interior $\mathcal{X}^o$ of $\mathcal{X}$, there exists a continuous bijection $f : \mathcal{X} \to \mathcal{X}$ such that $p_X^* = p_{f(X)}^*$, $p_{f(X)}^*\left(f\left(x^{(in)}\right)\right) = p_X^*\left(x^{(out)}\right)$, and $p_{f(X)}^*\left(f\left(x^{(out)}\right)\right) = p_X^*\left(x^{(in)}\right)$.*

Let's first provide a sketch of proof. We rely on the transformation depicted in Figure 8, which can swap two points while acting in a very local area. If the distribution of points is uniform inside this local area, then this distribution will be unaffected by this transformation. In order to arrive at this situation, we use the uniformization method presented in Subsection 4.1, along with a linear function to fit this local area inside the support of the distribution (see Figure 9). Once those two points have been swapped, we can reverse the functions preceding this swap to recover the original distribution overall.

Proof. Our proof will rely on the following non-rigid rotation $f^{(rot)}$. Working in a hyperspherical coordinate system consisting of a radial coordinate $r > 0$ and $(D-1)$ angular coordinates $(\phi_i)_{i<D}$,

$$\forall d < D,\ x_d = r\left(\prod_{i=1}^{d-1}\sin(\phi_i)\right)\cos(\phi_d)$$
$$x_D = r\left(\prod_{i=1}^{D-2}\sin(\phi_i)\right)\sin(\phi_{D-1}),$$

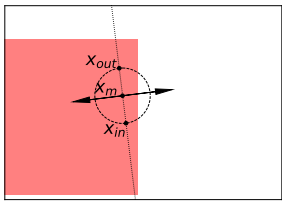

(a) When taking two points x_{in} and x_{out} inside the hypercube $[0,1]^D$, there is sometimes no L_2-ball centered in their mean x_m containing both x_{in} and x_{out}.

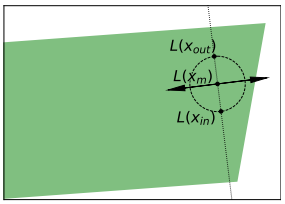

(b) However, given x_{in} and x_{out}, one can apply an invertible linear transformation L such that there exists a L_2-ball centered in their new mean $L(x_m)$ containing both $L(x_{in})$ and $L(x_{out})$. If the distribution was uniform inside $[0,1]^D$, then it is now also uniform inside $L\left([0,1]^D\right)$

Figure 9: We illustrate how, given x_{in} and x_{out} in a uniformly distributed hypercube $[0,1]^D$, one can modify the space such that $f^{(rot)}$ shown in Figure 8 can be applied without modifying the distribution.

where for all $i \in \{1, 2, ..., D-2\}$, $\phi_i \in [0, \pi)$ and $\phi_{D-1} \in [0, 2\pi)$, given $r_{max} > r_0 > 0$, we define the continuous mapping $f^{(rot)}$ as:

$$f^{(rot)}\big((r, \phi_1, \ldots, \phi_{D-2}, \phi_{D-1})\big) = \left(r, \phi_1, \ldots, \phi_{D-2}, \phi_{D-1} + \pi \frac{(r_{max} - r)_+}{r_{max} - r_0} [\text{mod } 2\pi]\right).$$

where $(\cdot)_+ = \max(\cdot, 0)$. This mapping only affects points inside $\mathcal{B}_2(0, r_{max})$, and exchanges two points corresponding to $(r_0, \phi_1, \ldots, \phi_{D-2}, \phi_{D-1})$ and $(r_0, \phi_1, \ldots, \phi_{D-2}, \phi_{D-1} + \pi)$ in a continous way (see Figure 8). Since the Jacobian determinant of the hyperspherical coordinates transformation is not a function of ϕ_{D-1}, $f^{(rot)}$ is volume-preserving in cartesian coordinates.

Let $f^{(KR)}$ be a Knothe-Rosenblatt rearrangement of p_X^*, $f^{(KR)}(X)$ is uniformly distributed in $[0, 1]^D$. Let $z^{(in)} = f^{(KR)}\left(x^{(in)}\right)$ and $z^{(out)} = f^{(KR)}\left(x^{(out)}\right)$. Since $f^{(KR)}$ is continuous, $z^{(in)}, z^{(out)}$ are in the interior $(0, 1)^D$. Therefore, there is an $\epsilon > 0$ such that the L_2-balls $\mathcal{B}_2\left(z^{(in)}, \epsilon\right)$ and $\mathcal{B}_2\left(z^{(out)}, \epsilon\right)$ are inside $(0, 1)^D$. Since $(0, 1)^D$ is convex, so is their convex hull.

Let $r_0 = \frac{1}{2}\left\|z^{(in)} - z^{(out)}\right\|_2$ and $r_{max} = r_0 + \epsilon$. Given $z \in (0, 1)^D$, we write $z_\parallel$ and $z_\perp$ to denote its parallel and orthogonal components with respect to $\left(z^{(in)} - z^{(out)}\right)$. We consider the linear bijection L defined by

$$L(z) = z_\parallel + \epsilon^{-1} r_{max} z_\perp.$$

Let $f^{(z)} = L \circ f^{(KR)}$. Since L is a linear function (i.e., with constant Jacobian), $f^{(z)}(X)$ is uniformly distributed inside $L\left([0, 1]^D\right)$. If $z^{(m)}$ is the mean of $z^{(in)}$ and $z^{(out)}$, then $f^{(z)}(\mathcal{X})$ contains $\mathcal{B}_2\left(L\left(z^{(m)}\right), r_{max}\right)$ (see Figure 9). We can then apply the non-rigid rotation $f^{(rot)}$ defined earlier, centered on $L\left(z^{(m)}\right)$ to exchange $L\left(z^{(in)}\right)$ and $L\left(z^{(out)}\right)$ while maintaining this uniform distribution.

We can then apply the bijection $\left(f^{(z)}\right)^{-1}$ to obtain the invertible map $f = \left(f^{(z)}\right)^{-1} \circ f^{(rot)} \circ f^{(z)}$ such that $p^*_{f(X)} = f^*_X$, $p^*_{f(X)}\left(f\left(x^{(in)}\right)\right) = p^*_X\left(x^{(out)}\right)$, and $p^*_{f(X)}\left(f\left(x^{(out)}\right)\right) = p^*_X\left(x^{(in)}\right)$. □

B A single-pixel counter-example

We generate 5^6 individual pixels as three-dimensional vectors according to a distribution built as follows: let $p_w = \mathcal{U}([255, 256]^3)$ (corresponding to the color white), $p_b = \mathcal{U}([0, 10]^3)$ (corresponding to shades of black), and $p_{out} = \mathcal{U}([10, 11]^3)$ (corresponding to a dark shade of grey), the pixels follow the distribution

$$p_X(x) = (1 - \beta)\big(\alpha \cdot p_w(x) + (1 - \alpha) \cdot p_b(x)\big) + \beta \cdot p_{out}(x),$$

where $\alpha = 1001^{-3}$ and $\beta = 10^{-4}$. Once generated, we concatenate these pixels in a 125×125 RGB bitmap image in Figure 10 for a more convenient visualization.

Visually, a common intuition would be to consider white pixels to be the anomalies in this figure. However, following a construction similar to Subsection 4.2, the final densities corresponding to pixels from p_w (equal to $\alpha(1 - \beta)$) and p_b (equal to $(1 - \alpha)(1 - \beta)10^{-3}$) are equal to $1001^{-3}(1 - 10^{-4}) \approx 10^{-3}$, and the final density corresponding to pixels from p_{out} (equal to β) is 10^{-4}. Therefore, none of the methods presented in Subsection 2.2 (density scoring) and Subsection 2.3 (typicality) would consider the white pixels (in $[255, 256]^3$) as outliers. They would only classify the pixels of a particular dark shade of grey in $[10, 11]^3$ as outliers.

Figure 10: We generated 5^6 pixels according to the procedure described in **??** and concatenate them in a single 125×125 RGB bitmap image for an easier visualization. While, visual intuition would suggest that white pixels are the outliers in this figure, density-based definitions of anomalies described Subsection 2.2 (density scoring) and Subsection 2.3 (typicality) would consider a specific dark shade of grey to be the outlier.